Conservative and dissipative tip-sample interaction forces probed with dynamic AFM

B. Gotsmann,* C. Seidel, B. Anczykowski, and H. Fuchs
Physikalisches Institut, Universität Münster, D-48149 Münster, Germany
(Received 31 March 1999)

The conservative and dissipative forces between tip and sample of a dynamic atomic force microscopy (AFM) were investigated using a combination of computer simulations and experimental AFM data obtained by the frequency modulation technique. In this way it became possible to reconstruct complete force versus distance curves and damping coefficient versus distance curves from experimental data without using fit parameters for the interaction force and without using analytical interaction models. A comparison with analytical approaches is given and a way to determine a damping coefficient curve from experimental data is proposed. The results include the determination of the first point of repulsive contact of a vibrating tip when approaching a sample. The capability of quantifying the tip-sample interaction is demonstrated using experimental data obtained with a silicon tip and a mica sample in UHV. [S0163-1829(99)01839-1]

I. INTRODUCTION

The tiny forces between a nanometer sized probe and sample have been intensively examined since the advent of atomic force microscopy (AFM). As there are numerous applications of AFM to a wide range of surfaces, the forces involved need to be understood in order to give a quantitative interpretation of AFM images. Furthermore, the analysis of the forces is relevant beyond AFM itself: the physics of nanometer sized particles or a tip and their interaction with surfaces are of interest to the fields of cluster physics, environmental science, the fabrication of nanostructures etc.

A variety of different theoretical models describing the tip-sample interaction were published previously: approaches based on continuum theory take into account attractive forces due to van-der-Waals interaction,[1] electrostatic interaction,[2] elasticity,[3] and can be set together to contact models with both attractive and repulsive forces (see, for example, the review by Krüger *et al.*[4]) Atomistic theories have also been applied.[5,6] All AFM techniques are sensitive to these forces, but only few of them are capable of determining the forces as a function of the separation between a probing tip and a sample. Contact AFM force-distance measurements with soft cantilevers can record the forces of the tip-sample interaction accurately. However, due to a mechanical instability when approaching a surface, a jump-to-contact of the probing tip occurs[7] when the force gradient becomes larger than the spring constant of the free cantilever. This prevents the determination of the full tip-sample potential. On the other hand, for cantilevers stiff enough to avoid this jump-to-contact there is a loss of sensitivity.[8]

In large amplitude dynamic AFM this jump-to-contact is avoided by using stiff cantilevers. The cantilever is vibrated at amplitudes much larger than the interatomic spacing (typically 1-100 nm). Here, the measurement of the corresponding ac signals can be very sensitive. Due to the reduction of friction and lateral forces during the scanning process damage to the tip or surface is minimized. All the advantages have been impressively demonstrated in a large number of recent publications showing atomically resolved images of reactive,[9,10] inert[11] as well as electrical insulating[12] surfaces and molecularily resolved images of thin organic adsorbate layers.[13,14] Often in these examples only attractive forces were involved and the FM technique[15] was applied using large amplitudes. This technique is chosen here to analyze and quantify tip-sample forces, but our results can also be applied to other AFM techniques.

In contrast to the case of extremely small vibration amplitudes,[16] the theoretical analysis of large amplitude dynamic AFM is not straightforward. It is not trivial to assign the acting forces to the images,[17] because the forces for each position of the tip represent a spacial integral of the pressure acting on the extensions of the tip. In addition, usually only the time averaged quantities of the moving tip (amplitude, frequency, etc.) are measured experimentally. This means that an integral over one period of vibration has to be considered. Further, for a given position of the cantilever support the tip moves through a large part of the tip-sample potential during each oscillation cycle, and as the potential is nonlinear the mathematical description is a nonlinear problem.

A force spectroscopy curve can be measured by varying the cantilever support distance from the sample while probing properties of the oscillation such as the frequency, amplitude, or phase. These dynamic force spectroscopy curves exhibit a strong material contrast[18,19] indicating a sensitivity to local mechanical properties, which has strong implications for possible applications. How can the corresponding curves then be related to forces? A large number of publications addresses the problems under various circumstances. The choice of the appropriate mathematical description depends on the different modes of operation. While for the amplitude-modulation (AM) technique (also called intermittent contact mode or slope detection) numerical methods are predominant,[4] rather good analytical descriptions[20] exist for the FM technique. In this report, however, a numerical method is used for the analysis of the FM technique, because of its applicability to any type of force. For example the simulation allows a reconstruction of the full force curve even in the case of discontinuous curves, as can occur, for example, on reactive surfaces.[21] Furthermore, the simulation turns out to be capable of also including energy dissipation

effects, which were not considered in previously published methods.

A property of dynamic AFM often neglected is that not only elastic (static) forces are probed but also dissipative (velocity dependent) forces may play a role. These forces can lead to strong material contrasts and are relevant to the interpretation of phase imaging in tapping mode AFM.[22,23] Similarly, in FM-AFM material contrasts can be obtained[12] and—as shown below—can be analyzed quantitatively. This opens up a new field of surface analysis for the quantitative determination of material properties on the nanometer scale. However, some of the underlying mechanisms, such as viscoelasticity are strongly frequency dependent—and in AM- or FM-AFM the frequency varies only marginally around the free resonant frequency of the AFM cantilever. Other scanning probe methods such as scanning acoustic microscopy[24] may not be restricted to one specific frequency.

In the presence of both, conservative and dissipative forces, it is desirable to analyze underlying mechanisms and distance dependencies in order to relate the results to other applications in the field of scanning probe microscopy.

II. EXPERIMENT

All presented experimental data were obtained under ultrahigh vacuum conditions using a commercial instrument (Omicron UHV AFM/STM), applying the FM-AFM technique.[15] Commercial silicon cantilevers with integrated tips (Nanosensors) were used (resonant frequency around 300 kHz, spring constant approximately 40 N/m). In the FM technique the driving signal of the cantilever excitation (performed by a small piezo plate) is generated through a feedback loop. The detector, sensing the cantilever movement, produces an ac signal, which is amplified, phase shifted, and then used as an excitation signal. The amplification is adjusted by a PI controller to keep the vibration amplitude constant. The frequency f of the vibrating lever then varies in response to the tip-sample interaction forces. The force induced shift of the resonant frequency Δf in the self-excited loop is used as a control signal to keep the tip-sample distance constant while scanning.

Dynamic force spectroscopy (DFS) with the FM technique is the recording of the two distance-dependent variables Δf and the gain factor R (proportional to the driving amplitude A_{exc}) as a function of the displacement of the cantilever support towards the sample d. Furthermore, for quantitative measurements the absolute value of the amplitude A, the Q value of the cantilever far away from the surface and the spring constant k_l have to be determined. The curves were recorded at preselected points of the surface, which can be explored by standard imaging. The reproducibility was checked by repeating the measurements. Plastic deformations of the tip or the sample can be detected by a persistent change in the spectroscopy curves.

In the example given below, the PI controller kept the amplitude constant to better than 99%. It is important to check this point experimentally because even deviations of only a few percent from the set amplitude A_0 can have measurable effects on the force spectroscopy curves. For example, softer PI controller settings can be chosen to improve the signal-to-noise ratio. It can even be advantageous to allow the amplitude to decrease slightly due to dissipation forces by choosing the values of the PI controller appropriately. In this case the situation would be more similar to the constant excitation FM technique.[25] The probability of tip wear or damage may then be reduced. However, for dynamic force spectroscopy a strong decrease of the amplitude is undesirable for two reasons: Firstly, regions of the potential of relatively strong repulsion and dissipation may not be reached by the tip at all, because further penetration of the tip is avoided by a faster reduction of the amplitude. Secondly, the effects of conservative and dissipative forces on the DFS curves are more difficult to seperate[26] if the amplitude is allowed to decrease rapidly with distance. From the theory of a simple harmonic oscillator one would expect that in the FM technique f responds to elastic forces (force gradients) while the excitation amplitude A_{exc} responds to dissipative forces. In the AM technique and in constant-excitation FM-AFM, however, this separation cannot be made so easily. In both the constant-excitation FM technique and the AM technique the excitation amplitude A_{exc} is kept constant while the vibration amplitude A is allowed to decay as a result of the forces acting between tip and sample. This implies that for *analytical purposes* of the forces the (constant vibration-amplitude) FM technique is more straightforward, and for *imaging* the constant excitation-amplitude techniques (AM-AFM and constant-excitation-FM-AFM) are favorable due to the avoidance of tip wear. Still, the complex situation must not be simplified too much at this point, especially as all different techniques have been proven equally powerful in imaging.[10,25]

III. THEORETICAL TREATMENT

In order to interpret the experimental force spectroscopy curves a mathematical description of the measurement process has to be found which leads to an expression in terms of conservative and dissipative tip-sample interaction forces. In this section only conservative forces are considered. Energy dissipation will be included in Sec. IV.

The vibration of the lever can be treated as a one dimensional movement. This assumptions holds for weak pertubations of the cantilever movement by tip-sample interaction,[24] which is usually the case in dynamic AFM. In the case of stronger tip/sample interaction as used in scanning acoustic microscopy[24] higher flexural modes of the cantilever vibration have to be taken into account. Further, the free lever behaves like a harmonic oscillator, i.e., the bending force of the lever follows Hook's law. Although, the theory of elasticity predicts a dependence of the force of the fourth-order spatial derivative of the lever deflection, Sarid[27] has shown that for very small deflections as present in AFM Hook's law can be restored. With these two assumptions the force based equation of motion yields:

$$m_{eff}\ddot{z}(t)+\beta_l\dot{z}(t)+k_l z(t)+F_{ts}[d+z(t)]=F_{exc}(t), \quad (1)$$

where z denotes the deflection of the cantilever, m_{eff} its effective mass, β_l the damping coefficient of the cantilever motion, and k_l the spring constant. The tip-sample interaction force is denoted by F_{ts} as a function of the absolute

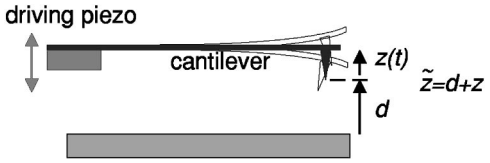

FIG. 1. Scheme, explaining the meaning of the variables z (the deflection of the lever), d (the lever support distance), and $\tilde{z}=z+d$ the absolute tip-sample separation.

tip-sample separation $\tilde{z}=d+z$ (see Fig. 1). F_{exc} describes the excitation through an actuator-piezo element. Corresponding to our experimental setup F_{exc} can be expressed by a mathematical description of a PI controller and feedback loop

$$F_{exc}(t)=R\cdot z(t-t_{phase}) \tag{2}$$

$$\text{with } R=p[A(t)-A_0]+i\int_{t'=0}^{t}[A(t')-A_0]\mathrm{d}t'$$

$$=r\left\{[A(t)-A_0]+\frac{1}{\tau_{pi}}\int_{t'=0}^{t}[A(t')-A_0]\mathrm{d}t'\right\}.$$

Here R denotes the loop-gain function. Experimentally, R can be measured as a function of d simultanously with $\Delta f(d)$. The actual vibration amplitude (peak-to-peak value) is denoted by $A(t)$, and A_0 is the corresponding set point value, p and i (or r and τ_{pi}) are the settings of the PI controller, t_{phase} is the phase shift. The inverse of t_{phase} is usually set to 3/4 of the actual frequency $f=f_0+\Delta f$, corresponding to a shift of $\pi/2$.

For our analysis we solved Eqs. (1) and (2) numerically, but in order to find an analytical or simpler numerical solution of this mathematical problem simplifications of these equations have been made in the literature. Three important cases of approximative forms [Eqs. (3), (5), and (8)] of the equation of motion will be discussed below.

It is straightforward to assume that such a self-excited system always vibrates at its mechanical resonance on which the excitation has no influence except for the chosen vibration amplitude. The role of the feedback circuit then is purely to compensate for energy losses, and hence both the excitation of the lever and the damping factor β_l are neglected. If, in addition, the interaction force is linearized over the range of the tip movement we find

$$m_{eff}\ddot{z}(t)+(k_l+k_{ts})\,z(t)=0, \tag{3}$$

$$\text{where } k_{ts}=\frac{\partial F_{ts}(d)}{\partial d}.$$

In this case, a complete and simple analytic expression can be found[15] for the frequency shift:

$$\Delta f(d)=\frac{f_0}{2k_l}k_{ts}(d) \quad \text{for } \Delta f\ll f_0. \tag{4}$$

The validity, however, is restricted to the case of very small vibration amplitudes.

By introducing a nonlinear but conservative tip-sample interaction force into the equation of motion

$$m_{eff}\ddot{z}(t)+k_l z(t)+F_{ts}[d+z(t)]=0 \tag{5}$$

the problem can be treated as a weakly perturbed harmonic oscillator. Giessibl[20] used a force of the form

$$F_{ts}(\tilde{z})=\sum_{n=1}^{\infty}\frac{C_n}{\tilde{z}^n}, \tag{6}$$

where the C_n are constants, and found for large vibration amplitudes

$$\Delta f(d)=-\frac{1}{\sqrt{2}\pi}\frac{f_0}{k_l A_0^{3/2}}\sum_{n=1}^{\infty}\frac{C_n\ I(n)}{(d-A_0/2)^{n-1/2}}, \tag{7}$$

$$\text{with } I(n)=\frac{\pi}{2^{n-1}}\prod_{i=2}^{n}\frac{2i-3}{i-1}.$$

This very useful equation was actually derived by perturbation theory from a Hamiltonian-function, which is not strictly equivalent to Eq. (5). The approximation (7) provides an understanding of the relation of Δf to the different measurement parameters k_l, A_0, and f_0 as well as the dependence on different force characteristics.[1,3] The exponent of the distance dependence in Eq. (7) is $n-1/2$ in strong contrast to $n+1$ in Eq. (4). This is because Eq. (7) is an approximation for large amplitudes while Eq. (4) is valid for small amplitudes.

Alternatively, Eq. (5) can be solved numerically[28] resulting in a handy and (numerically) very fast method, which is a convenient way even to simulate whole AFM images with similar or better accuracy as compared to Eq. (7). In contrast to the analytic solution given in Eq. (7), the time averaged deflection of the lever due to the mean force can be taken into account by a numeric solution. In the following section (IV A) the solution given in Eq. (7) will be compared with the numerical simulation using the full ansatz of Eqs. (1) and (2).

A further step lies in taking into account the excitation of the cantilever. This can most easily be done by assuming a harmonic driving force

$$m_{eff}\ddot{z}(t)+\beta_l\dot{z}(t)+k_l z(t)+F_{ts}[d+z(t)]$$

$$=A_{exc}\cos(\omega_{exc}t). \tag{8}$$

Here, the excitation amplitude A_{exc} (in units of a force) is introduced, ω_{exc} is the driving frequency—an approximation for Eq. (2). Again, both analytic (Sasaki *et al.*,[29] or Boisgard *et al.*[30] derived with the Lagrange formalism) and numeric[29] solutions are possible. The vibration amplitude and phase lag can be determined as a function of the driving amplitude and driving frequency. The complete resonance curves obtained hereby are relevant for the interpretation of both the AM and the FM technique. For the interpretation of $\Delta f(d)$-curves obtained with the FM technique the resonance condition has to be found with the requirement that the vibration amplitude A is equal to its set point A_0. This makes the numerical effort quite similar to solving Eqs. (1) and (2) directly. A simple solution similar to Eq. (7) cannot be given for Eq. (8). The resonance curves obtained by solving Eq. (8) exhibit strong distortions from the simple harmonic case when a strong

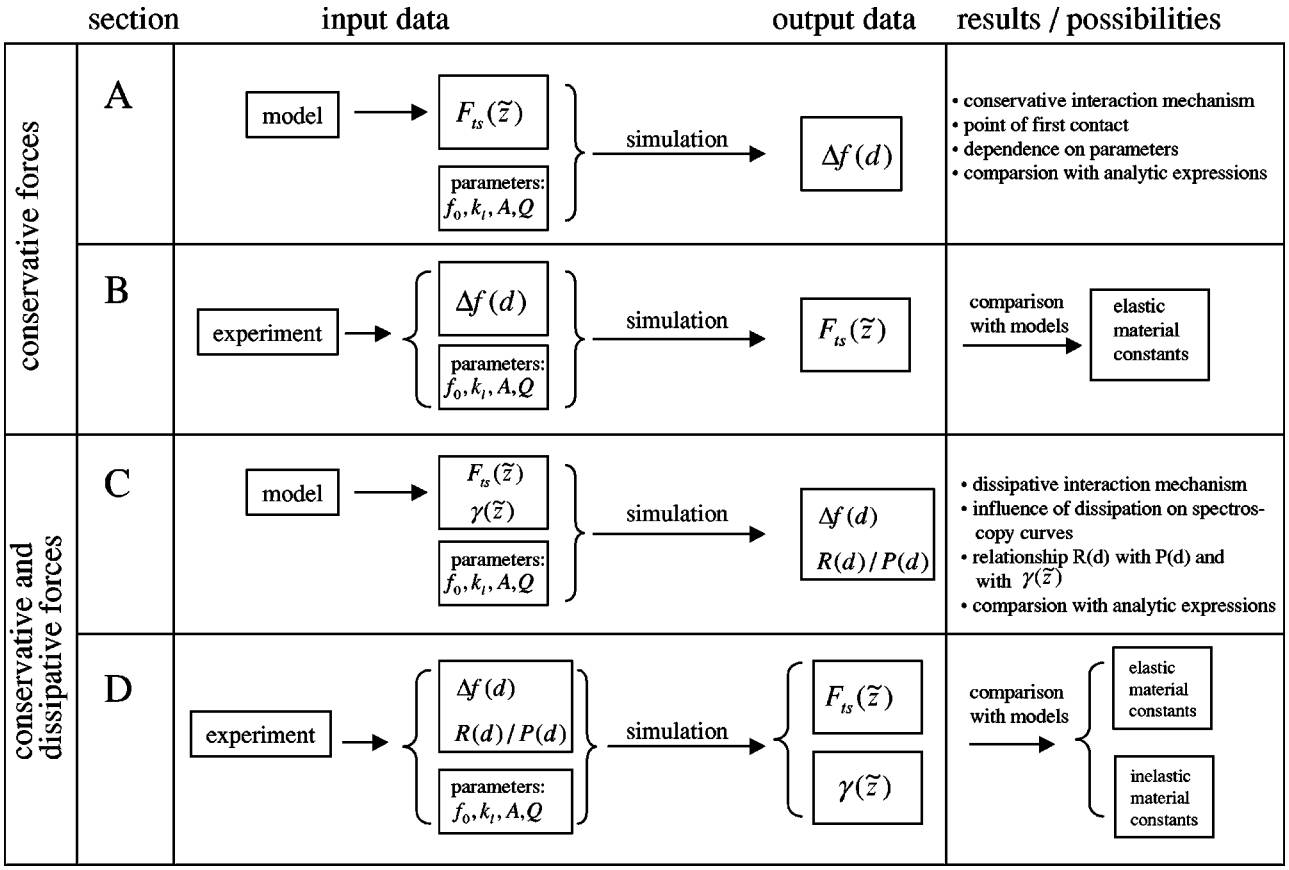

FIG. 2. Schematic overview of the cases involved in the different sections.

force interaction is involved. This is in agreement with experimental observations.[31–33] Hysteresis effects can be seen depending on the direction of the frequency sweep, the maximum of the amplitude curve becoming flat. Hence, bistabilities appear in the resonance curves and, depending on how this bistability is accounted for, results can vary[29] in theoretically calculated DFS curves.

In the experiment using the FM technique the self-excited feedback loop guarantees that the lever always vibrates at its mechanical resonance. The definition of resonance for a standard driven harmonic oscillator is the maximum of the resonance curve, which is equal to a phase lag of $\pi/2$. Under the influence of nonlinear interaction forces, however, the resonance condition is more complicated. The phase lag between excitation and vibration is fixed by the feedback loop and determines the resonance condition. This becomes important when distorted resonance curves appear. Hence, the analysis using Eq. (8) promises a deeper understanding of the complicated situation.

Regarding all the different examples listed above, we find a whole range of theoretical approaches to choose from for further analysis. Clearly, with increasing complexity of the equation of motion the corresponding solutions become less intuitive. The analytical approaches given in Eqs. (4) and (7) allow a clear insight into the dependence of the frequency shift on different parameters. The apparent drawback of clumsy simulation approaches is counterbalanced by their extreme flexibility. In fact, different types of forces can be introduced easily, such as dissipative forces, discontinuous forces, or adhesion hysteresis. As the complete trajectory $z(t)$ is obtained by simulation, it is possible to analyze anharmonicity, contact times (see also Tamayo *et al.*[22]), etc. Furthermore, the model assumptions can be reduced to a minimum.

Therefore, we choose to solve Eq. (1) directly including the form of a PI controller as in Eq. (2). In our simulation the values of the PI controller have been selected to reproduce the behavior of the experimental setup. They are about $p = 10^{-4}$ N/m, $i = 0{,}06$ N/(ms), leading to a time constant of $\tau_{pi} = 1.67^{-3}$ ms. The differential equation was solved using the Verlet algorithm.[34] All input parameters can be determined experimentally: A_0, k_l, β, f_0, p, and i. Hence, the spectroscopy curves $\Delta f(d)$ and the corresponding force curves $F_{ts}(\tilde{z})$ can be related to each other with no further assumptions and no fit parameters.

IV. RESULTS AND DISCUSSION

In the four following sections, different cases are considered, which are illustrated in Fig. 2. In Sec. IV A, a *conservative model force* is fed into the simulation. Based on *experimental* $\Delta f(d)$ data a force vs distance curve is calculated quantitatively with the help of the simulation in Sec. IV B. In Sec. IV C, again, a *model force* is used but this time *energy dissipation* is included. Finally, in Sec. IV D *experimentally* determined energy dissipation rates are used for a quantitative determination of the *dissipative forces* alongside conservative forces.

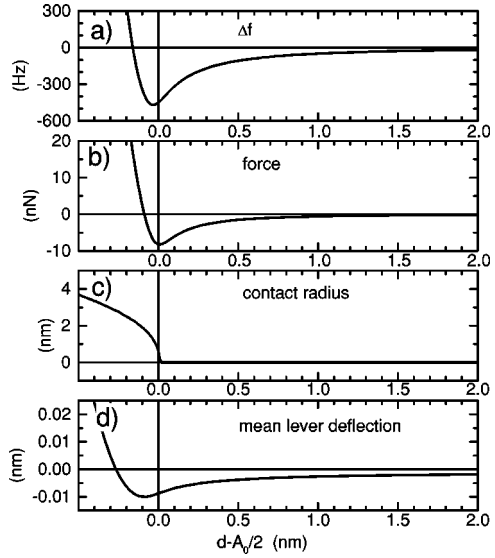

FIG. 3. Computer simulation using Eqs. (1) and (2) with the parameters: $f_0=300$ kHz, $A=20$ nm (peak-to-peak), $Q=20\,000$ and $k_l=40$ N/m. The force stems from the MYD/BHW-model for $A_H=3\times10^{-19}$ J (Hamaker constant), $\nu=0.42$ (Poisson ratio), $E=1.74\times10^{11}$ Pa (elastic modulus of tip and sample) and $R_{tip}=20$ nm in a sphere-plate geometry. (a) Calculated $\Delta f(d)$-curve, (b) force acting between tip and sample at the reversal point of the oscillation cycle for each d, (c) contact radius at lower inflection point, (d) mean deflection of the lever (time averaged). The d axis was shifted by $A_0/2$ giving the absolute tip-sample distance at the inflection point approximately.

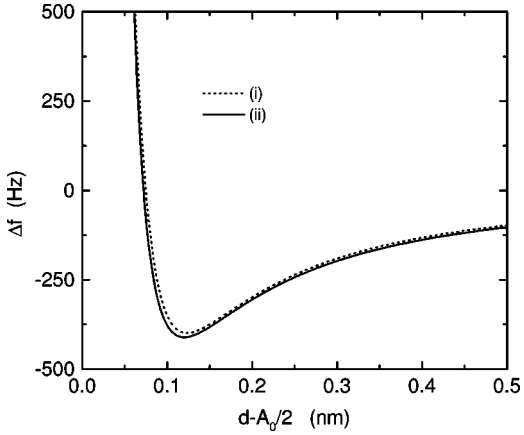

FIG. 4. $\Delta f(d)$ curve calculated by numerical simulation (i) and analytically with Eq. (7) (ii). The parameters are the same as in Fig. 1. The force is given in the text.

A. Model calculations: Conservative forces

A result of the simulation with a conservative model force is given in Fig. 3. The tip-sample interaction force curve is taken from the Muller, Yushenko, Dergaguin/Burgess, Hughes, White (MYD/BHW) model.[35] This model is based on continuum theory considering long-range attractive and repulsive contact forces. For the numeric evaluation of the force curve the pressure distribution between tip and sample was derived from a Lennard-Jones potential. The elastic response of tip and sample was also considered. The total force is then calculated by integration of the pressure function over the tip area.[4]

Typical experimental values were chosen as input parameters for the simulation of the spectroscopy curve. Solving the equation of motion (1) and (2) for these values leads us to a $\Delta f(d)$-curve as depicted in (a). The general shape of known experimental curves can clearly be recognized. The simulation, however, allows an extraction of much more information about the system.

At first, the force that acts between the tip and the sample at the reversal point of the oscillation cycle as a function of d is plotted in Fig. 3(b). This allows us to assign set point values of Δf (chosen for scanning surfaces) to the forces acting. For the interpretation of the forces it is important to know the contact radius in addition to the mere value of the forces, because the force for a given separation of tip and sample is given through integration of the pressure acting on different parts on the tip.[4] The forces acting on the tip *apex* are most important for the imaging process while attractive contributions of the rest of the tip form a background. For the interpretation of the imaging process it is therefore important to separate absolute forces and repulsive forces acting on the asperity only.[17] This can be done by simultaneously plotting the contact radius which might be extracted from the evaluation of the model force.

Our example shows that the transition from attractive to repulsive total forces takes place on the branch of increasing values of Δf (with respect to approach of the tip to the sample),[36] whilst the transition to repulsive forces on the asperity of the tip (indicated by a contact radius greater than 0) already takes place on the branch of decreasing values of $\Delta f(d)$ [see Fig. 3(c)]. It is thus not appropriate to assign an operation in the regime of falling values of $\Delta f(d)$ to pure attractive forces. Our results are in agreement with calculations by Hölscher *et al.*,[28] although their calculation was based on a different tip-sample interaction force and integration method. Hence, we do not expect strong deviations of this result when using other model forces for the tip-sample contact (e.g., a force derived from atomistic theory with a van-der-Waals background).

In addition to the force, the mean deflection of the cantilever, as obtained by averaging the oscillation signal in time, is plotted in Fig. 3(d). For the chosen magnitude of force amplitude and spring constant the absolute deflection values remain marginal. For an analytical approach this indicates that we need to consider the mean deflection as a small correction only.

The curves plotted (in this case of pure elastic forces) do not depend on the chosen values of the PI controller once the preset amplitude is reached and kept constant. We also checked for the influence of the parameters Q, A_0, k_l, and the discretion of the time variable Δt. We found that there is virtually no dependence of the resulting curve on Q (or β_l). The dependence on A_0 and k_l matches the predictions of Giessibl[20] within a few per cent for sufficiently large amplitudes. Δt has to be chosen greater than $1/(500f_0)$. It ranges from $1/(1000f_0)$ to $1/(4000f_0)$ in our examples.

Finally, we compare our results to the analytical formula given in Eq. (7). The result is shown in Fig. 4. As a trial force we chose $F_{ts}(\tilde{z})=C_2\tilde{z}^{-2}+C_3\tilde{z}^{-3}$ with $C_2=5\times10^{-28}$ m^{2}N and $C_3=4.8\times10^{-38}$ m^{3}N, which is of the form of Eq. (6) and hence, Eq. (7) can be applied. The difference in terms of absolute numbers seems to be rather large

(some percent in the region far from the surface and some ten percent near the surface), but when looking at the two curves in Fig. 4 we find a rather good qualitative agreement between the numerical method using Eqs. (1) and (2) and the analytical expression given by Eq. (7). In contrast to this, the solution (4) is far from giving a comparable result.

B. Determination of force distance curves from experimental frequency shift curves

In the paragraphs above we only considered the case where a conservative force curve is given from which a $\Delta f(d)$ curve was calculated. However, the experiment provides only $\Delta f(d)$ curves, while the determination of corresponding $F_{ts}(\tilde{z})$ is desired. The calculation of $F_{ts}(\tilde{z})$ from measured $\Delta f(d)$-curves—the *inverse* problem–is the key to the quantitative analysis of DFS. This is a further aspect of the choice of an appropriate theoretical model which has not been mentioned above (in Sec. III). Except for the analytical solution in Eq. (4) there is no straightforward way to solve this inverse problem. One possibility is to use an expansion into a power series with Eq. (6) and numerical fitting of the $\Delta f(d)$-curves using (7). The numerical solution of Eqs. (1) and (2) can also be used with an algorithm based on the iteration of the variation of $F_{ts}(\tilde{z})$ until the simulated $\Delta f(d)$ curve matches the experimental one. We developed a special algorithm,[19] which allows us to perform such a calculation with our simulation method in a relatively time saving way (only five to ten times the calculation time required for the noninverse problem). As in similar mathematical problems a numerical variation method is applied: a trial force curve $F_{ts}(\tilde{z})$ is chosen, a $\Delta f(d)$ curve calculated, from the deviation of the resulting $\Delta f(d)$ curve with respect to the experimental one a new trial force curve is derived and so on. Our algorithm is optimized by omitting the variation of whole force curves. Instead the independent variable d is divided into small steps Δd. This discretion is undertaken anyhow in the experimental procedure, hence, no information is lost in comparison with the experimental input data $\Delta f(d)$. Furthermore, even discontinuous $\Delta f(d)$ curves, which have already been observed experimentally,[21,36] can be used in the simulation method.

The force curves are determined without any model assumptions concerning the properties of the tip-sample interaction force. All input parameters and the force spectroscopy curve $\Delta f(d)$ can be readily determined from the experiment, and there are no fit parameters necessary to obtain a complete $F_{ts}(\tilde{z})$ curve. For the *interpretation* of the resulting force curves, however, in terms of Hamaker constants, elastic moduli, etc. contact models and tip shapes have to be taken into account. For example: the repulsive part of the calculated force curve can be fitted with a curve expected from the Hertz-model.[3] Examples of different experimental curves of various surfaces are given in a previous paper.[19]

An example for the calculation is given in Fig. 5. We took an experimental $\Delta f(d)$ curve [Fig. 5(a)], which was obtained on a mica surface. The calculated force curve is shown in Fig. 5(b). It is a complete curve which exhibits the long-range attractive part as well as the short-range repulsive part. We fitted the attractive region and found the best fit using a distance dependence $\tilde{z}^{-2}$, which corresponds to a sphere-plate approximation of van-der-Waals forces. We used the well known equation[3] $F_{vdW}(\tilde{z})=A_H R_{tip}/(6\tilde{z}^2)$ and a tip radius of $R_{tip}=20$ nm (manufacturer information). From this we obtained a Hamaker constant of $A_H=1.2\times10^{-19}$ J ($\pm50\%$) in agreement with our expectations for the two kinds of material involved.[3] Introducing the same tip radius now into the best fit for the repulsive branch with $F_{Hertz}(\tilde{z})=(-\tilde{z})^{3/2}R_{tip}/K$ (Hertz model) gives us a reduced elastic modulus $K=10^{10}$ Nm^{-2}($\pm100\%$), which is of the expected order of magnitude. However, the applicability of the Hertz model is limited in this case due to the fact that mica has no homogenous elasticity.

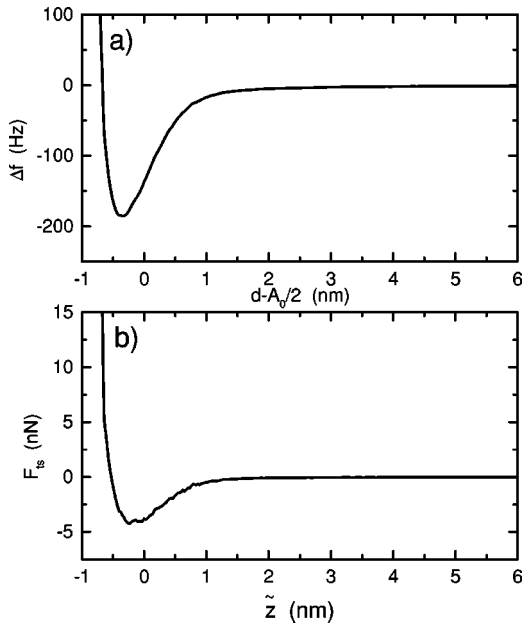

FIG. 5. The experimental $\Delta f(d)$ curve is given in (a) and the calculated $F_{ts}(\tilde{z})$ curve is given in (b). As the amplitude is kept constant the normalized axis $d-A_0/2$ for (a) corresponds to $\tilde{z}$ in (b) identical with the force acting at the lower inflection point. The measurement/simulation parameters are: $f_0=296\,593$ Hz, $A_0=32$ nm (peak-to-peak), $Q=22815$, and $k_l=40$ N/m. The simulation was carried out with an accuracy of 0.05 Hz with regard to the experimental $\Delta f(d)$ curve (smoothed) and a step width $\Delta d=2.7\times10^{-11}$ m.

For both fits the choice of the origin ($d=0$) becomes relevant. The experiment and the simulation can give only relative measures of the tip-sample displacement, the absolute tip-sample separation can only be estimated up to an accuracy of about 2×10^{-10} m in this case. The choice of the origin in the chosen example was made through analogy with contact models[4] and led to the best fits to the models.

With the example it becomes clear that the quantitative analysis of DFS has a high-analytic potential. By determining all properties of tip and sample, which are experimentally accessible (elastic constants, tip shape, contact potential difference, etc.) it might even be possible to examine the contact models themselves, as the calculation method to determine $F_{ts}(\tilde{z})$ is independent of specific model assumptions.

C. Model calculations including energy dissipation

Let us now include dissipative tip-sample forces in our consideration. Although in dynamic AFM the tip usually

moves at apparently ''slow'' velocities (less than 1 m/s), dissipative forces leading to energy loss of the movement are a very important factor in the tip-sample interaction.

In a first order approach one can regard our system as a sinusodially driven simple harmonic oscillator. Then we expect for small damping effects that damping merely influences the amplitude of the vibration, or in the FM technique the excitation amplitude necessary to keep the vibration amplitude constant. In this model the frequency shift is only influenced by conservative forces. This separation of elastic and dissipative forces is to be verfied in this section.

The mathematical expression for energy dissipation or dissipation forces depends on the underlying mechanism. For small velocities we chose a simple form

$$F_{ts}^{diss}(\tilde{z},\dot{z}) = \gamma(\tilde{z}) \cdot \dot{z}, \tag{9}$$

where the force is a function of the absolute position between tip and sample and proportional to the cantilever velocity. This ansatz is justified for many different dissipation mechanisms such as electronic dissipation[37] or simplified models of viscoelasticity of the sample[22] but becomes more complex if adhesion hysteresis, capillary hysteresis,[38] or more complicated descriptions of viscoelasticity[39] are included.

In a model calculation we simulated a $\Delta f(d)$ curve, as we did in the pure elastic case, with the same conservative model force, but now assumed an additional dissipative force of the form of Eq. (9) with

$$\gamma = \gamma_{0exp} \exp(-\tilde{z}/z_0), \tag{10}$$

γ_{0exp}, and z_0 being constants. This ansatz of the damping coefficient for the experimental situation describes the decay of the dissipative force with distance when tip and sample are out of contact, and at the same time reflects the rise of damping effects with increasing repulsive contact. The result of the simulation is depicted in Fig. 6 where $\Delta f(d)$, $A(d)$, the time averaged dissipation power $\overline{P(d)}$ and $A_{exc}(d)$ are plotted. The corresponding curves for the case without energy dissipation were given in Fig. 3. By comparing Fig. 3(a) and Fig. 6(a) we find that there is only little influence of the energy dissipation on the $\Delta f(d)$-curves. The small influence can be accounted mainly to the small decrease of amplitude (up to 0.2%) through energy dissipation and can be neglected in this case. However, for cases of larger dissipation rates and cases where the settings of the PI controller allow a stronger decrease of the amplitude, the influence of energy dissipation on the frequency shift has to be considered—a topic of further investigation. The dissipation rate shown here is of the order of experimental data obtained with the AM technique on silicon.[23] However, we expect a larger dissipation rate on polymer samples[18] especially when using the FM technique.

In order to determine the dissipation power from experimental data it is possible to use some fundamental equations as used also for intermittent contact mode AFM by Cleveland *et al.*[23] and Anczykowski *et al.*[18] modified for the FM technique. We find for the power dissipated by the tip-sample interaction averaged over one period of vibration

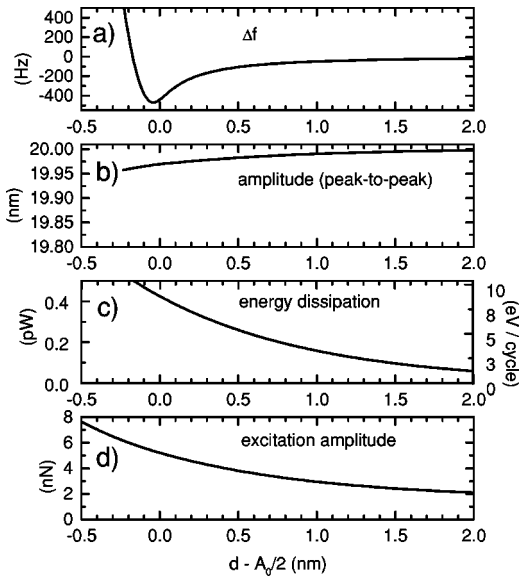

FIG. 6. Computer simulation using Eqs. (1) and (2) with the same parameters and the same force as in Fig. 3 but with an additional dissipative force (given in the text): (a) $\Delta f(d)$ curve, (b) $A(d)$-curve, (c) energy dissipation (rate) curve $P(d)$, and (d) excitation amplitude curve $A_{exc}(d)$.

$$\overline{P(d)} = \frac{\pi k f(d) A^2(d)}{4Q}\left[\frac{R(d)}{R_0} - \frac{f(d)}{f_0}\right], \tag{11}$$

where R_0 is the gain factor for the cantilever far away from the surface. In this equation, we use the gain factor $R(d)$ [see Eq. (2)] rather than the excitation amplitude. This is because with regard to the signal-to-noise ratio in the experiment it is easier to calculate the excitation amplitude by multiplying the gain factor with the vibration amplitude of the lever than to measure it directly. The formula can be easily checked by applying it to the simulation data in Fig. 6. In the simulation the actual dissipation power

$$P(t) = F_{ts}^{diss}[z(t),\dot{z}(t),d] \cdot \dot{z}(t), \tag{12}$$

is to be averaged over one period of the oscillation. The deviation of the curve determined with Eq. (11) from the curve determined directly in the simulation [Fig. 6(c)] is less than 0.05%. This indicates that Eq. (11) can also be applied to experimental data. In simulations not shown here we found that Eq. (11) can even be used to calculate the energy losses due to adhesion hysteresis effects. In the case of adhesion hysteresis effects being present we would expect a different qualitative behavior in the experimental curves from the ones shown in this report. At the point where the adhesion hysteresis is generated for the first time within a dynamic force spectroscopy curve, a discontinuity in the $\overline{P(d)}$ curve should occur. At the same time the $\Delta f(d)$ curve, which would show an averaged effect of approach and retraction force curve, should not be mathematically differentiable. Careful experiments are needed to adress the analysis of adhesion hysteresis in more detail.

In the example (Fig. 6) the damping coefficient function $\gamma(\tilde{z})$ is related to the dissipation function $\overline{P(d)}$ by means of the computer simulation. An expression for $\overline{P(d)}$ can also be derived analytically with appropriate approximations. The

actual dissipation power [Eq. (12)] has to be averaged over one period of the oscillation. Assuming a harmonic movement, this calculation can be carried out analytically for a dissipative force as given in Eqs. (9) and (10), and we find (see Appendix A)

$$\overline{P(d)} = I_1\left(\frac{A_p}{z_0}\right) A_p z_0 \omega^2 \gamma_{0exp} \exp\left(-\frac{d}{z_0}\right), \qquad (13)$$

where I_1 is the modified Bessel function of first order. The approximation given in Eq. (13) was compared quantitatively with the simulation [Fig. 6(c)] and an agreement of better than 98% was found.

D. Determination of conservative and dissipative forces from experimental data

Finally, we consider the case where DFS curves are given experimentally while conservative and dissipative forces are to be determined. As the effects of conservative and dissipative forces are only weakly coupled (see Sec. IV C), a variation method similar to the one described above for the pure elastic calculation (see Sec. IV B) can be applied.

As an example we consider again the measurement on a mica sample (Fig. 5). The experiment provided a curve for $R(d)$, which was recorded simultaneously with $\Delta f(d)$, and from these curves a damping coefficient function $\gamma(\tilde{z})$ is to be determined. As a first step, the $R(d)$ curve can be translated into a curve of the dissipation power $\overline{P_{diss}(d)}$ using Eq. (11). Then, this $\overline{P_{diss}(d)}$ curve can be related to a dissipation coefficient $\gamma(\tilde{z})$ in a similar way as described above for the calculation of the conservative $F_{ts}(\tilde{z})$ from $\Delta f(d)$ (Sec. IV B). As the corresponding algorithm may become numerically unstable it is desirable to have an approximate trial function $\gamma(\tilde{z})$ determined by an analytical method or an independent numerical algorithm.

Assuming a harmonic movement of the cantilever and a dissipative force of the form of Eq. (9) the problem can be solved analytically, if γ is of the form of Eq. (10) or of the form:

$$F_n^{diss}(\tilde{z},\dot{z}) = \gamma_n(\tilde{z}) \cdot \dot{z}$$

$$\text{with} \quad \gamma_n(\tilde{z}) = \frac{\gamma_{0n}}{(\tilde{z})^n}, \quad n = 0,1,2,\ldots \ .$$

The results are given in Appendix A providing explicit formulas for the corresponding functions $\overline{P_n(d)}$, $n=0,1,2,\ldots$. However, these functions are difficult to handle for a series expansion. Therefore, a simple numeric approach outlined in Appendix B was chosen here to determine the desired trial function $\gamma(\tilde{z})$ from the $\overline{P(d)}$ curve. The corresponding dissipative force was inserted into our simulation and the calculation of $F_{ts}(\tilde{z})$ from $\Delta f(d)$ was done as described above, but this time the energy dissipation was calculated simultaneously. The $\gamma(\tilde{z})$ function was varied until the simulation reproduced the experimental $\overline{P(d)}$ curve satisfactorily.

As the energy dissipation is comparatively small there is only a negligible difference of the determined $F_{ts}(\tilde{z})$ curve when compared to the one in the purely elastic calculation. This is in accordance with the above results with weak energy dissipation (Sec. IV C), but might differ in other experimental situations.

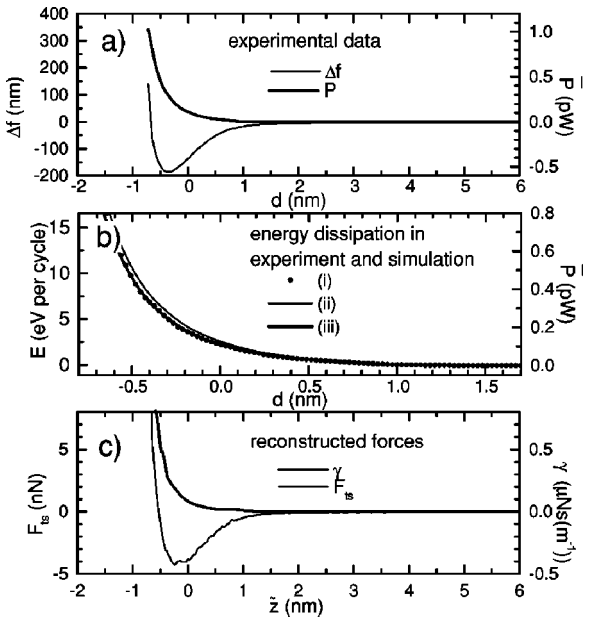

FIG. 7. Calculation based on the experimental data as used in Fig. 5 for a mica surface. The experimental $\Delta f(d)$ curve is given in (a) together with the experimental energy dissipation rate curve $P(d)$ [calculated using Eq. (11)]. In (b) $P(d)$ curves are given for the experimental case (i) (smoothed), the trial function obtained by the algorithm in Appendix B (ii), and the curve after variation (iii). In (c) the calculated force curves are plotted which were derived from the experimental data with the simulation method. The conservative force as well as the damping coefficient curve $\gamma(\tilde{z})$ [corresponding to (iii) in (b)] are shown.

The results of the calculation are shown in Fig. 7. In Fig. 7(a) the experimental data is shown [$\Delta f(d)$ and $\overline{P(d)}$]. In Fig. 7 (b) the experimental $\overline{P(d)}$ curve is shown together with a simulated one using a trial function for $\gamma(\tilde{z})$ from Appendix B and an optimized $\gamma(\tilde{z})$ curve. In Fig. 7(c) the calculated tip-sample interaction forces are shown, the conservative part $F_{ts}(\tilde{z})$ as well as the damping coefficient function $\gamma(\tilde{z})$, after variation. It is hereby shown that a quantitative calculation of conservative and dissipative forces from experimental data is possible. As can be seen from the calculated curves the damping coefficient rises rapidly when the surface is elastically deformed. Besides this strong damping in the contact regime a significant amount of damping takes place in the attractive region. This could originate in the creation of image charges in the tip induced by thermally fluctuating charges or residual static charges on the mica surface. Similarily to the conservative forces we expect the damping coefficient $\gamma(\tilde{z})$ to be a superposition of several contributions originating from different mechanisms.

Although better experimental data is needed for a more detailed analysis, the proposed technique opens the perspective of a quantitative analysis of dissipative forces and the underlying mechanisms.

V. SUMMARY

In summary, dynamic force spectroscopy (DFS) based on the FM technique can be used for the quantitative analysis of the tip-sample interaction forces, which is a step towards the absolute evaluation of material properties and the verification of tip-sample interaction models. Computer simulations of the cantilever movement enable us to relate interaction forces to frequency shifts and, in addition, energy dissipation rates.

With the use of model calculations (Sec. IV A) the point of first contact on approaching the oscillating probe to the surface was determined to be close to the minimum of the $\Delta f(d)$ curve. This is in strong contrast to predictions based on simplified models stating that $\Delta f(d)$ is proportional to the force gradient. An analytic formula given by Giessibl[20] leads to a good agreement with the simulation.

With the reconstruction method (Sec. IV B) complete conservative force-distance curves were determined without fit parameters. Possible applications lie in the verification of contact models or the quantitative determination of material constants such as the elastic modulus or the Hamaker constant. The latter carries information specific for the material. An example is given for a mica sample.

The energy dissipation can easily be calculated from the experimental data with a simple analytic formula Eq. (11), which was verified by the simulation (Sec. IV C). The dissipation rate is of interest for the experimentalist to estimate the influence of the tip on the sample and vice versa. Energy dissipation is introduced into the simulation using model data (Sec. IV C) and experimental data (Sec. IV D). It is shown that the entanglement of conservative and dissipative forces in terms of their mutual effect on frequency shifts and loop gain factors is small in the examples given. However, generalization for cases of much larger dissipation rates require further investigation.

To relate the experimental energy dissipation rates to position dependent damping coefficient functions $\gamma(\tilde{z})$ different methods can be applied. For some general forms of the $\gamma(\tilde{z})$-function analytic expressions of the dissipation rate are derived (Appendix A). An approximate $\gamma(\tilde{z})$ function can be calculated using a simple numeric algorithm (Appendix B). This algorithm can be applied to more complicated forms of $\gamma(\tilde{z})$-functions. Finally, using the computer simulation a quantitative determination of this damping coefficient function is possible by a reconstruction method (Sec. IV D) similar to the one used for conservative forces.

As an example, a $\gamma(\tilde{z})$ function was determined from experimental data obtained on a mica sample (Sec. IV D). The example shows that a quantitative analysis of energy dissipation is possible even in the regime of purely attractive forces. From this a comparison with theoretical models is possible, allowing us to evaluate corresponding material constants.

To conclude, DFS can now be used for the quantitative evaluation of material properties and the interpretation of AFM images. Thus DFS may establish a method for the determination material constants such as Hamaker constants, electronic conductance (through electrostatic forces and through electronic energy dissipation), viscoelastic constants, elastic moduli and others, alongside with imaging surfaces at ultimate resolutions.

ACKNOWLEDGMENTS

It is a pleasure to thank D. Krüger, D. Pohl, U. D. Schwarz, H. Hölscher, and U. Freking for fruitful discussions and encouragement.

APPENDIX A: ANALYTIC WAY TO OBTAIN $\gamma(\tilde{Z})$

The energy dissipation rate as a function of the DFS parameters is calculated for simple forms of damping coefficient curves $\gamma(\tilde{z})$.

For a dissipative force of the form

$$F_n^{diss}(\tilde{z},\dot{z}) = \gamma_n(\tilde{z})\cdot\dot{z}$$

$$\gamma_n(\tilde{z},d) = \frac{\gamma_{0n}}{(\tilde{z})^n},\quad n=0,1,2,\ldots$$

we find for the energy dissipation rate

$$P(t) = F_n^{diss}[z(t),\dot{z}(t),d]\cdot\dot{z}(t).$$

Assuming a harmonic cantilever movement

$$z(t) = A_p\cos\omega t$$

$$\dot{z}(t) = -\omega A_p\sin\omega t$$

we can now calculate the mean dissipation power by solving the integral

$$\overline{P(d)} = \frac{\omega}{2\pi}\int_0^{2\pi/\omega}|P(t)|\,dt = \frac{\omega}{\pi}\int_0^{\pi/\omega}\frac{\gamma_{0n}(-\omega A_p)^2\sin^2\omega t}{(d+A_p\cos\omega t)^n}dt$$

$$= \frac{\omega^2}{\pi}A_p^{2-n}\,\gamma_{0n}\int_0^{\pi}\frac{\sin^2 x}{\left(\frac{d}{A_p}+\cos x\right)^n}dx.$$

This integral can be solved analytically, for $n>1$ we find[40]

$$\overline{P(d)} = \omega^2 A_p^{2-n}\,\gamma_{0n}\frac{(-2)^{n-1}}{1-n}\frac{a^{n-2}}{(a^2-1)^{2n-3}}\cdot\sum_{\nu=0}^{n-2}\binom{n-1}{\nu}$$

$$\times\binom{2n-4-\nu}{n-2}(a^2-1)^{\nu},$$

where we introduced a:

$$a = \frac{d}{A_p}+\sqrt{\frac{d^2}{A_p^2}-1}.$$

For $n=0$, we have explicitly

$$\overline{P(d)} = \frac{\omega^2\gamma_{00}A_p^2}{2},$$

which is equivalent to the intrinsic damping of the cantilever [compare with Eq. (11)], and

$$\overline{P(d)} = \omega^2 \gamma_{01} \frac{A_p}{a} = \omega^2 \gamma_{01} \frac{A_p}{\dfrac{d}{A_p} + \sqrt{\dfrac{d^2}{A_p^2} - 1}} \quad \text{for} \quad n=1,$$

$$\overline{P(d)} = \omega^2 \gamma_{02} \left(\frac{\dfrac{d}{A}}{\sqrt{\dfrac{d^2}{A_p^2} - 1}} - 1 \right) \quad \text{for} \quad n=2.$$

The solution of simple power laws of the form

$$F_n^{diss}(\tilde{z},\dot{z}) = \gamma_{0n} \cdot (\tilde{z})^n \cdot \dot{z}, \quad n=0,1,2,\ldots$$

can be obtained accordingly[40] also resulting in a closed expression, but it is more useful to look at a dissipative force of the form

$$F_{exp}^{diss}(\tilde{z},\dot{z},d) = \gamma_{0exp} \cdot \exp\left(-\frac{\tilde{z}}{z_0} \right) \cdot \dot{z},$$

where z_0 is the decay length. Here we find a mean dissipation power of

$$\overline{P(d)} = I_1\left(\frac{A_p}{z_0}\right) A_p z_0 \omega^2 \gamma_{0exp} \exp\left(-\frac{d}{z_0} \right). \tag{A1}$$

I_1 is the modified Bessel function of first order.

APPENDIX B: NUMERIC WAY TO OBTAIN $\gamma(\tilde{z})$

In this appendix the energy dissipation rate as a function of the DFS parameters is calculated numerically for any form of damping coefficient curves $\gamma(\tilde{z})$.

The experimental force spectroscopy curve is given in steps i. We can then define

$$f_i = f_0 + \Delta f(d_i)$$

$$\text{with} \quad d = d_0 - i \cdot \Delta d, \quad i = 0,\ldots,m.$$

The entire movement of the tip can be regarded seperately on the intervals

$$(d_0 - A/2 - j\Delta d) < \tilde{z} < [d_0 - A/2 - (j-1)\Delta d], \quad j = 1,2,\ldots m.$$

A denotes the peak-to-peak value of the oscillation amplitude. If the function $\gamma(\tilde{z})$ is defined as constant on these small intervals

$$\gamma(\tilde{z}) = \gamma_j$$

$$\text{for } (d_0 - A/2 - j\Delta d) < \tilde{z} < [d_0 - A/2 - (j-1)\Delta d],$$

$$j = 1,2,\ldots m \tag{B1}$$

then the dissipation power on this interval can be approximated by

$$P_{ij} = \frac{\gamma_j \Delta d^2}{(\Delta t_{ij})^2}, \tag{B2}$$

$$\text{where} \quad t_{ij} = \frac{1}{2\pi f_i} \arcsin\left[\frac{A/2 - (i-j)\Delta d}{A/2} \right] i \geq j \geq 0$$

$$\text{and} \quad \Delta t_{ij} = t_{i(j+1)} - t_{ij}.$$

For the time averaged dissipation power we find:

$$\overline{P(d_i)} = 2 f_i \sum_{j=0}^{i-1} P_{ij} \Delta t_{ij} = 2 f_i \sum_{j=0}^{i-1} \gamma_j \frac{(\Delta d)^2}{\Delta t_{ij}},$$

which can be solved for γ_i successively for $i = 1,2,\ldots m$.

This method produces a trial function $\overline{P(d)}$ only. The approximation in Eqs. (B1) and (B2) are not used in the simulation described in Secs. IV C and IV D.

*Electronic address: gotsman@uni-muenster.de

[1] U. Hartman, Phys. Rev. B **43**, 2404 (1991).

[2] S. Belaidi, P. Girard, and G. Leveque, J. Appl. Phys. **81**, 1023 (1997).

[3] J. Israelachvili, *Intermolecular and Surface Forces, 2nd ed.* (Academic Press, London, 1992).

[4] D. Krüger, B. Anczykowski, and H. Fuchs, Ann. Phys. (Leipzig) **6**, 341 (1997).

[5] R. Perez, M. C. Payne, I. Stich, and K. Terakura, Phys. Rev. Lett. **78**, 678 (1997).

[6] A. L. Shluger, L. N. Kantorovich, A. I. Livshits, and M. J. Gillan, Phys. Rev. B **56**, 15 332 (1997).

[7] R. Wiesendanger, *Scanning Probe Microscopy and Spectroscopy* (Cambridge University Press, Cambridge, 1994).

[8] G. Cross, A. Schirmeisen, A. Stalder, P. Grütter, M. Tschudy, and U. Dürig, Phys. Rev. Lett. **80**, 4685 (1998).

[9] F. J. Giessibl, Science **267**, 68 (1995).

[10] R. Erlandsson, L. Olsson, and P. Martensson, Phys. Rev. B **54**, R8309 (1996).

[11] W. Allers, A. Schwarz, U. D. Schwarz, and R. Wiesendanger, Appl. Surf. Sci. **140**, 247 (1999).

[12] M. Bammerlin, R. Lüthi, E. Meyer, A. Baratoff, J. Lü, M. Guggisberg, Ch. Gerber, L. Howald, and H.-J. Güntherodt, Probe Microscopy **1**, 1 (1997).

[13] B. Gotsmann, C. Schmidt, C. Seidel, and H. Fuchs, Eur. Phys. J. B **4**, 267 (1998).

[14] K-I. Fukui, H. Onishi, and Y. Iwasawa, Phys. Rev. Lett. **79**, 4202 (1997).

[15] T. R. Albrecht, P. Grütter, D. Horne, and D. Rugar, J. Appl. Phys. **69**, 668 (1991).

[16] S. P. Jarvis, H. Yamada, S.-I. Yamamoto, H. Tokumoto, and J. P. Pethica, Nature (London) **384**, 247 (1996).

[17] I. Y. Sokolov, G. S. Henderson, and F. J. Wicks, Surf. Sci. **381**, L558 (1997).

[18] B. Anczykowski, B. Gotsmann, H. Fuchs, and J. P. Cleveland, Appl. Surf. Sci. **140**, 376 (1999).

[19] B. Gotsmann, B. Anczykowski, C. Seidel, and H. Fuchs, Appl. Surf. Sci. **140**, 314 (1999).

[20] F. J. Giessibl, Phys. Rev. B **56**, 16 010 (1997).

[21] T. Uchihashi, Y. Sugawara, T. Tsukamoto, M. Ohta, S. Morita, and M. Suzuki, Phys. Rev. B **56**, 9834 (1997).

[22] J. Tamayo and R. Garcia, Appl. Phys. Lett. **71**, 2394 (1997).

[23] J. P. Cleveland, B. Anczykowski, A. E. Schmid, and V. B. Elings, Appl. Phys. Lett. **72**, 2613 (1998).

[24] U. Rabe, J. Turner, and W. Arnold, Appl. Phys. A: Mater. Sci. Process. **66**, S277 (1998).
[25] H. Ueyama, Y. Sugawara, and S. Morita, Appl. Phys. A: Mater. Sci. Process. **66**, S295 (1998).
[26] B. Gotsmann, B. Anczykowski, and H. Fuchs (unpublished).
[27] D. Sarid, *Scanning Force Microscopy with Applications to Electric, Magnetic and Atomic Forces* (Oxford University Press, New York, 1991).
[28] H. Hölscher, U. D. Schwarz, and R. Wiesendanger, Appl. Surf. Sci. **140**, 344 (1999).
[29] N. Sasaki and M. Tsukada, Jpn. J. Appl. Phys., Part 2 **37**, L533 (1998).
[30] R. Boisgard, D. Michel, and J. P. Aime, Surf. Sci. **401**, 199 (1998).
[31] P. Gleyes, P. K. Kuo, and A. C. Boccara, Appl. Phys. Lett. **58**, 2989 (1991).
[32] A. Kühle, A. H. Sorensen, and J. Bohr, J. Appl. Phys. **81**, 6562 (1997).
[33] W. Sabisch, G. Becker, and H. Fuchs, Probe Microscopy **1**, 259 (1998).
[34] L. Verlet, Phys. Rev. **159**, 98 (1967).
[35] V. M. Muller, V. S. Yushchenko, and B. V. Derjaguin, J. Colloid Interface Sci. **77**, 91 (1980); A. K. Burgess, B. D. Hughes, and L. R. White (unpublished).
[36] B. Gotsmann, D. Krüger, and H. Fuchs, Europhys. Lett. **39**, 153 (1997); , **41**, 583 (1998).
[37] W. Denk and D. Pohl, Appl. Phys. Lett. **59**, 2171 (1991).
[38] O. P. Behrend, F. Oulevey, D. Gourdon, E. Dupas, A. J. Kulik, G. Gremaud, and N. A. Burnham, Appl. Phys. A: Mater. Sci. Process. **66**, S219 (1998).
[39] S. C. Hunter, J. Mech. Phys. Solids **8**, 219 (1960).
[40] W. Gröbner and N. Hofreiter, *Integraltafel*, 4th edition (Springer-Verlag, Wien, Berlin, 1966), Vol. II.